ASME Journal of Electrochemical Energy Conversion and Storage
Online journal at:
https://asmedigitalcollection.asme.org/electrochemical

Modeling the Inhomogeneous Stress Distribution in Proton Exchange Membrane Gas Diffusion Layers Taking Into Account Fiber Substrate and Microporous Layer

Felix Benz
Institute for Electrochemical Process Engineering, IET-4,
Forschungszentrum Jülich,
Jülich 52428, Germany;
Foundry Institute,
RWTH Aachen University,
Aachen 52066, Germany
e-mail: f.benz@fz-juelich.de

Proton exchange membrane fuel cells and electrolyzers rely on carbon fiber gas diffusion layers (GDLs) for effective reactant transport, water management, and mechanical support. The mechanical integrity behavior of the carbon fiber substrate and the microporous layer (MPL) is critical during assembly due to compression-induced stresses. In this brief, a coupled mechanical model is used that captures the inhomogeneous stress and displacement distributions in the fiber/microporous layer composite structure under compression. The fiber substrate is modeled using 1D beam theory, while the MPL is represented through a 3D finite element method. An artificial composite structure is generated based on microstructural parameters. The model captures localized deformation and stress concentration phenomena consistent with experimental observations. Results reveal that the inhomogeneities in mechanical stiffness due to fiber clustering and MPL intrusion into fiber pores can play a significant role in the overall cell mechanics. This work advances the understanding of GDL's mechanical behavior and offers insights into improving fuel cell performance and longevity through more robust component design. [DOI: 10.1115/1.4071097]

Keywords: electrolyzers, fuel cells, novel numerical and analytical simulations

1 Introduction

Proton exchange membrane (PEM) fuel cells have emerged as a promising energy conversion technology due to their high efficiency, low operating temperature, and potential for sustainable hydrogen-based energy solutions. A critical component of these fuel cells is the gas diffusion layer (GDL). The GDL provides a transition between the macroscopic flowfield and the microscopic reaction sites at the electrodes. It enables the transport of reactant gases, provides water distribution management, and gives mechanical support to the membrane-electrode assembly. Typically, the GDL consists of a carbon fiber paper with an additional microporous layer (MPL) coated onto the fiber substrate. During cell assembly, the cell components are pressed together. Yim et al. [1] and Irmscher et al. [2] experimentally varied the applied pressure during the assembly process and reported a correlation between the applied pressure on the active area of the cell and the cell performance. As the GDL is the most compressible component in the cell, the stress and displacement distributions in the cell are greatly influenced by the GDL mechanical properties [3]. Inhomogeneous stress distributions during compression are inevitable due to the porous nature of the GDL. During cell assembly, this stress distribution is applied to other cell components and sets high demands on, e.g., the mechanical integrity of the membrane [4]. So far, the magnitude of the stress peaks arising in the GDL is not well understood. Previous studies by Le Carre et al. [5], Lee and Yang [6], and García-Salaberri et al. [7] have focused on the channel land pattern of the flowfield as a source for inhomogeneities. However, the porous GDL itself is also a major source of inhomogeneities leading to stress peaks. Understanding the mechanical behavior of the GDL and the stress arising during the compression of the cell is a key factor in optimizing the overall durability and performance of PEM fuel cells and can mitigate potential risks of mechanical membrane failure.

In recent years, the GDL mechanics have been subject to increased interest. The experimental stress–strain curve of GDLs with and without MPL has been measured by Carral and Mélé [8]. They reported a complex compression behavior of the composite material. Analytical models of the composite fiber/MPL GDLs have been proposed by Afrasiab et al. [9]. However, the material was treated as homogeneous, and no distinction between the fiber substrate and MPL was made.

Microscopic fiber structure modeling has been used by Norouzifard and Bahrami [10]. Here, an analytical model for the compression stress–strain curve based on beam theory is derived. Zhang et al. [11] and Lu et al. [4] simulated the random fiber structures of paper-type GDL using a 3D finite element method (FEM) approach. Sun et al. report a strong inhomogeneous stress distribution in the fiber structure of gas diffusion layers based on such a 3D reconstructed FEM simulation [12].

Previous research on microscopic GDL mechanics has focused on the fiber substrate used in GDLs. However, the MPL is expected to significantly alter the mechanics. This study focuses on the deformation behavior under compression of the fiber substrate and MPL. Understanding the interactions between these layers is crucial for optimizing GDL and membrane design, preventing membrane piercing, and improving overall system efficiency. In the case of mass transport simulations, the MPL has already been included in microscopic models. The porous structure of the fiber substrate and its porosity distribution are reported by Odaya et al. [13]. Banerjee and Bazylak [14] created an artificial micropore distribution for pore network models including the MPL pores. Fazeli et al. [15] performed pore network calculations on reconstructed GDL/MPL layers. To create the MPL material, they applied a morphological image opening technique, taking into account the pores of the fiber substrate.

A mechanical modeling approach is described to characterize the fiber/MPL composite, extending a previously described fiber model [16] with a coupled FEM model of the MPL. An artificial domain is generated with parameters such as fiber density and

Manuscript received June 10, 2025; final manuscript received August 26, 2025; published online February 24, 2026. Assoc. Editor: Partha P. Mukherjee.

MPL thickness based on X-ray tomography (CT) images. To describe the fiber substrate, a randomly generated fiber structure is used. The MPL domain is based on the random fiber structure with MPL material protruding into the pores of the fiber substrate. The mechanical model used consists of a beam theory model used for the fiber structure, a linear mechanical FEM model for the MPL, and a coupling scheme between the fiber substrate and the MPL. The model is simple enough to compute large domains covering multiple pores of the fiber substrate. The model can be used to evaluate the GDL/MPL behavior under compression as occurring during fuel cell assembly. By advancing knowledge in GDL mechanics, this research aims to contribute to the development of more robust and efficient PEM fuel cells for widespread commercial applications. Strategies to improve the mechanical resilience of cell components can be found.

2 Theory

2.1 Structure Creation. Both fiber substrate and MPL are typically not well-defined materials, but their material structure has a random component. The fibers in the fiber paper follow a random orientation distribution in the plane. An approach to generate an artificial fiber structure was proposed by Thiedmann et al. [17] and applied in Ref. [16] for mechanical modeling of GDL fiber structures. Following this approach, a random fiber structure is created in a cylindrical domain. The fibers are assumed to have infinite length and are oriented in the x, y plane with uniform fiber orientation distribution in the plane. All fibers are horizontal in the undeformed state. The fibers have equidistant z positions between the upper and lower fiber substrate boundaries. The number of fibers generated is determined by the porosity of the GDL's fiber substrate.

During the production process, the MPL is coated onto the fiber substrate. As a result, a pure MPL layer and a mixed MPL fiber layer, where MPL protrudes into the pores of the fiber substrate, are formed. In this work, the MPL domain is generated with the following procedure illustrated in Fig. 1(*a*): The domain of the MPL layer and the mixed layer is completely filled with material. The material inside the fibers is removed from the MPL. Above fibers, the MPL material in a cone of angle α is removed. The lower half of the fiber is considered to be in contact with the MPL. Fibers completely surrounded by the MPL material do not occur. The entire fiber and MPL domain are shown in Fig. 1(*b*).

2.2 Fiber Substrate Model. The fiber substrate model proposed by Benz [16] is used. As proposed by Norouzifard and Bahrami [10], beam bending theory is used to calculate the deflection $\omega(x)$ along the fibers as a function of the bending force $q(x)$:

$$IE\frac{\partial^4\omega}{\partial x^4} = q(x) \tag{1}$$

with elastic modulus E and second moment of area I. A linear spring model as described in Ref. [16] is added to take the binder material into account. This adds a force F to fibers i, j that are in proximity, where $r_{i,j}$ is the distance between the two fiber segments, l_i is the segment length, $b_{i,j}$ is the binder width, and θ is the angle to the compression direction.

$$F^i_{z,B} = E_B\frac{l_i b_{i,j}}{r_{i,j}}\frac{z_i - z_j}{r_{i,j}}(\omega_i - \omega_j)\cos(\theta) \tag{2}$$

Each fiber of the randomly generated fiber structure is discretized into equidistant segments. Intersecting fiber segments i,j are considered mechanically coupled with equal displacement ω.

$$\omega_i = \omega_j \tag{3}$$

The deflection of segments not in contact with other fibers is defined by the discretized beam equation:

$$EI\left(\frac{\omega_{i-2} - 4\omega_{i-1} + 6\omega_i - 4\omega_{i+1} + \omega_{i+2}}{\Delta x^4}\right) \tag{4}$$

On the side boundary, the slope of the fibers is set to zero.

$$\left.\frac{\partial\omega}{\partial x}\right|_{\text{Boundary}} = 0 \tag{5}$$

In the case of damage to fibers and binder, the maximum occurring stress in the fiber and binder material is checked after each simulation step. If the stress occurring in a fiber or binder segment exceeds a maximum stress, the segment is considered broken at this point and is removed from the simulation.

2.3 Microporous Layer Model. The elastic modulus of the MPL is determined by compression experiments of the MPL material coated onto a 20 μm thin copper foil. Multiple layers of MPL material and copper foil are stacked and compressed in a mechanical testing station. A stress–strain curve is recorded. As copper has a much higher stiffness than the MPL material and the total thickness of the copper is small, the deformation of the copper foil is insignificant compared to the deformation of the MPL. A linear fit between the stress and the strain is performed for different deformation regions. Available MPL samples are too thin to experimentally measure the Poisson ratio. It is assumed that $\nu = 0$, which is a reasonable approximation for porous materials.

The isotropic St Venant–Kirchhoff material model is used for modeling the MPL material. The stress in the reference configuration

$$\mathbf{S} = \mathbf{C}:\mathbf{E} \tag{6}$$

is given by the constant stiffness tensor $\mathbf{C}$ and the Lagrangian Green strain $\mathbf{E}$.

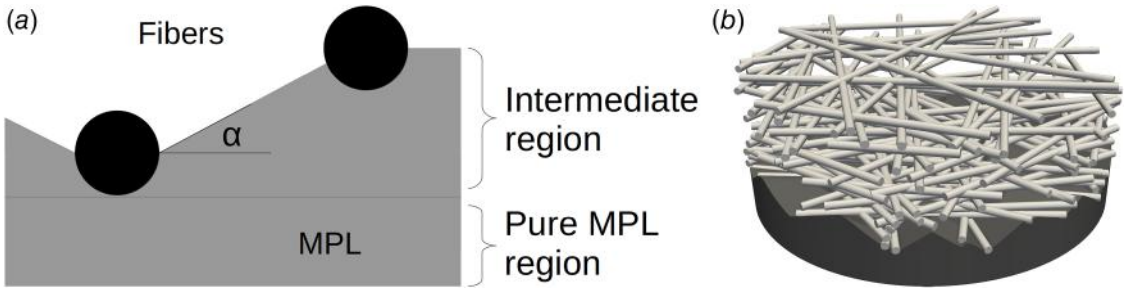

Fig. 1 (*a*) Sketch of the MPL creation. A pure MPL layer is present below the fiber substrate. In the intermediate layer, both fibers and MPL are present. The MPL intrudes into the pores of the fiber substrate. Areas above fibers are left empty. The slope of the MPL intrusion into the fiber substrate pores is given by the angle α. (*b*) Simulation domain of fibers on the top and MPL on the bottom. The fibers are discretized in 1D along the fiber direction. The MPL is discretized into 3D polyhedral cells.

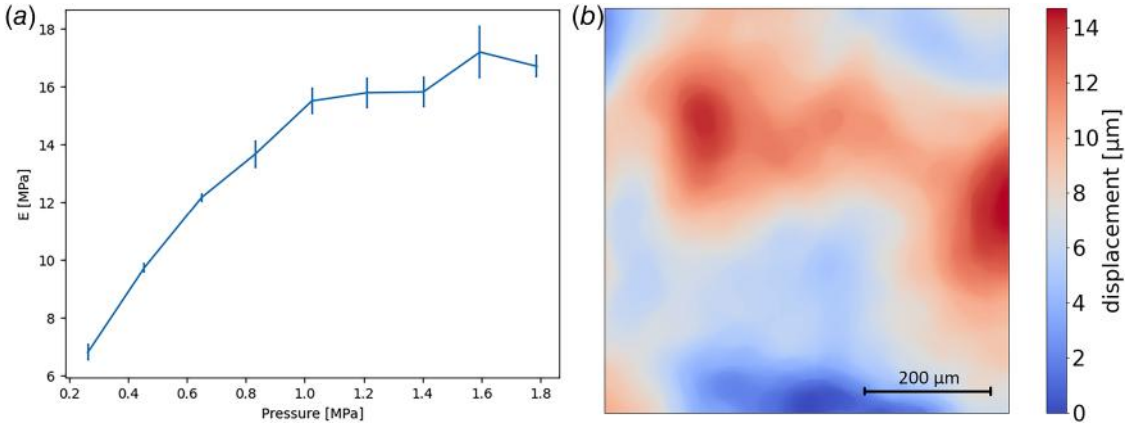

Fig. 2 (*a*) Elastic modulus of the MPL material on a copper foil as a function of compression pressure and (*b*) displacement on the membrane/MPL interface from CT

The coefficients of $\mathbf{C}$ are determined by the elastic modulus E and the Poisson ratio ν of the MPL material. The solids4Foam library [18] is used to solve the mechanical equations in the MPL domain. The boundary of the MPL consists of four different boundary types: The faces in contact with the fiber structure are subject to coupling with the fibers. Here, the displacement of the fibers is used as a boundary for the differential equations. The faces on the top side of the MPL not in contact with any fiber are subject to a zero force boundary. This does not change throughout the simulation, and additional contact points between MPL and fibers are not considered. The sides of the MPL are subject to a symmetry boundary. The displacement component perpendicular to the side boundary and the force component in the other two directions are fixed to zero. The bottom or the outside of the MPL has a fixed pressure boundary. The pressure is fixed to a constant value over the boundary. The pressure value depends on the simulation step.

The yield strength of Nafion is less than 1 MPa at typical cell conditions of 80 °C and fully water-saturated material [19]. Since the typical clamping pressure in a cell is higher, it can be assumed that the membrane material flows until a constant equilibrium pressure is reached throughout the interface.

2.4 Coupling Procedure. The interface between the fiber substrates consists of all MPL boundary faces touching a fiber segment and the corresponding fiber segments. The MPL mesh is finer than the fiber mesh. Multiple MPL faces can be in contact with a fiber segment. MPL faces are always coupled to a single fiber segment. Friction, contact breaking, and additional contacts are not considered. The boundary map between the fiber substrate and MPL remains throughout the simulation.

An iterative coupling scheme is used. The mechanical equations in the MPL are solved with a fixed displacement boundary condition on the interface. The deflections on the MPL faces i are given by the coupled fiber segment n.

$$\boldsymbol{\omega}_{\mathrm{MPL},i} = \boldsymbol{\omega}_{\mathrm{fiber},n} \tag{7}$$

In the next iteration, the force arising on the interface is used as a boundary condition for the fiber substrate.

$$\boldsymbol{f}_{\mathrm{fiber},n} = \sum_i \boldsymbol{f}_{\mathrm{MPL},i} \tag{8}$$

The mechanical equations for the fiber substrate are solved with the external force from the MPL, and the displacement on the interface is passed on to the MPL and used as a boundary condition. To account for the difference in the stiffness of the fiber substrate and the MPL, an implicit stiffness term is added to fiber segments in contact with the MPL:

$$q_{\mathrm{impl}} = (d_i - d_{i-1}) \sum_i K_i \tag{9}$$

This term does not affect the result of the simulation but improves numerical stability. For the data transfer between the fiber and the MPL simulation, the software PRECISE is used [20].

3 Results

3.1 Experimental. Figure 2(*a*) shows the elastic modulus of the MPL material as a function of the compression pressure. The depicted compression pressure is in the domain of typical assembly pressures relevant for fuel cell and electrolyzer applications [2]. The stiffness of the MPL increases with increasing compression. During compression, MPL cracks present in the uncompressed state as well as the MPL pores are closed, leading to a more dense material and higher mechanical stiffness. For higher compression ratios above 0.1, the elastic modulus reaches a plateau of about 16 MPa.

For simplicity, only a single value is used for the elastic stiffness in the model. The changes in the material properties are neglected, and a mean value of 12 MPa is used throughout the whole compression range.

A stack consisting of two GDLs with MPL and a Nafion membrane of 25 μm is compressed between two flat stamps, and images are recorded via CT imaging for two different compression steps. The assembly of the stack and the recording is done at room temperature and 50% relative humidity, and the membrane is in a dry state. At the interface between the membrane and the MPL, a step in the X-ray absorption can be seen. The interface is identified in both compression steps, and the displacement of the interface between the compression steps is calculated. Figure 2(*b*) shows the displacement in the compression direction at one interface between MPL and the membrane. A characteristic waviness can be seen. During compression, the inhomogeneous material stiffness of the GDL leads to different local displacements. Areas where the top GDL has a higher stiffness than the bottom GDL are pushed down and vice versa. The imprints of individual fibers cannot be seen on the MPL/membrane interface.

3.2 Simulation. A random fiber structure was created on a cylindrical domain of radius $R = 180\ \mu$m and height $H = 80\ \mu$m. The MPL structure corresponding to this fiber arrangement was calculated. A simulation was carried out on this domain. The simulation parameters are taken from Ref. [16]: The fiber and binder elastic moduli are $E_F = E_B = 230$ GPa, the fiber diameter

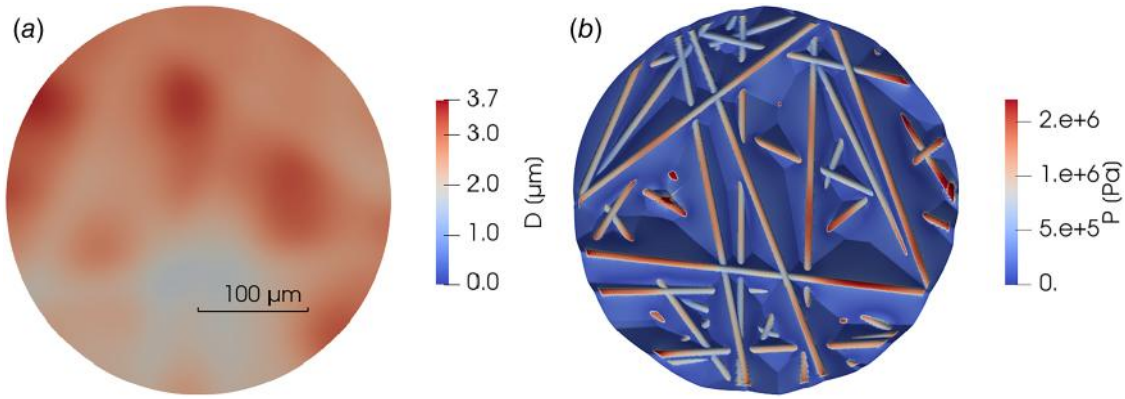

Fig. 3 Results of the simulation without fiber damage: (*a*) predicted displacement on the outside of the MPL and (*b*) predicted stress distribution on the fiber/MPL interface

is $D_F = 7\ \mu$m, the cutoff distance for the binder is $r_{max} = 17\ \mu$m, and the maximum strain is $\varepsilon_{max} = 0.015$. The fiber density is $V_F = 0.1$, and the binder density is $V_B = 0.02$.

The applied pressure on the bottom boundary patch is set to $P = 0.3$ MPa, and the deformation of the composite is calculated. The resulting displacement on the outside of the MPL is depicted in Fig. 3(*a*). The displacement shows an inhomogeneous distribution with a height difference of 1.9 μm between the maximum and the minimum displacement. Multiple localized displacement peaks can be seen. The spatial extent of the inhomogeneities corresponds to a typical pore size in the fiber structure. The autocorrelation length, i.e., the length at which the autocorrelation function drops below ½, is calculated to be 130 μm for the displacement on the bottom boundary. This is in a similar length scale as the autocorrelation length of 91 μm observed in the CT images. In the CT data, the displacement on the membrane boundary is a superposition of the microstructure from two GDL pressed onto the membrane from both sides, while the displacement observed in the simulation is only caused by one GDL microstructure. This can partially explain the lower autocorrelation length of the experiment in comparison with the simulation result. The stress distribution on the MPL/fiber interface is shown in Fig. 3(*b*). The stress is passed on to the fiber structure at local points and is not evenly distributed along the fibers. The stress passed from individual fibers to the MPL is not directly translated to displacement on the bottom of the MPL. While the MPL cannot compensate for all the inhomogeneities, fiber clusters with high stiffness cannot be compensated, and it acts as a buffer and can distribute the stress of single fibers.

A simulation with damage included in the GDL's fiber substrate model is carried out on the same structure. The reduced compression resistance of the fiber substrate leads to higher displacements. The difference between maximum and minimum displacement is 2.1 μm and is slightly larger than in the case without damage. The ability of the material to yield under high stress does not reduce the extent of the inhomogeneity in the compression behavior.

4 Conclusions

The compression stress experienced during cell assembly places significant mechanical demands on both the GDL and the membrane. Due to the porous nature of the GDL's fiber substrate, the resulting stress distribution is inherently inhomogeneous. To analyze this behavior, a simulation was performed using a combined approach: a 1D beam model for the fiber substrate and a 3D FEM model for the MPL. The simulation revealed inhomogeneous deformation patterns, consistent with observations from CT imaging of actual GDL/membrane stacks. These mechanical stiffness inhomogeneities, occurring on a length scale of approximately 100 μm, can be directly linked to the porous structure of the fiber network and fiber clusters with high mechanical stiffness.

Acknowledgment

The work presented in this article has been supported by AIDAS—AI, Data Analytics and Scalable Simulation—which is a joint virtual laboratory gathering by the Forschungszentrum Jülich (FZJ) and the French Alternative Energies and Atomic Energy Commission (CEA) and by the Deutsche Forschungsgemeinschaft (DFG, German Research Foundation)—491111487. The experimental GDL and MPL samples were provided by SGL Carbon in the framework of the QM-GDL project.

Conflict of Interest

There are no conflicts of interest.

Data Availability Statement

The datasets generated and supporting the findings of this article are obtainable from the corresponding author upon reasonable request.

References

[1] Yim, S.-D., Kim, B.-J., Sohn, Y.-J., Yoon, Y.-G., Park, G.-G., Lee, W.-Y., Kim, C.-S., et al., 2010, "The Influence of Stack Clamping Pressure on the Performance of PEM Fuel Cell Stack," Curr. Appl. Phys., **10**(2), pp. S59–S61.
[2] Irmscher, P., Qui, D., Janßen, H., Lehnert, W., and Stolten, D., 2019, "Impact of Gas Diffusion Layer Mechanics on PEM Fuel Cell Performance," Int. J. Hydrogen Energy, **44**(41), pp. 23406–23415.
[3] Bograchev, D., Gueguen, M., Grandidier, J.-C., and Martemianov, S., 2008, "Stress and Plastic Deformation of MEA in Fuel Cells: Stresses Generated During Cell Assembly," J. Power Sources, **180**(1), pp. 393–401.
[4] Lu, K., Lan, S., An, L., and Lin, R., 2024, "Mechanical Nonlinearity and Microscale Deformation of Gas Diffusion Layer in Proton Exchange Membrane Fuel Cell," J. Phys. Chem. C, **129**(1), pp. 962–972.
[5] Le Carre, T., Blachot, J.-F., Poirot-Crouvezier, J.-P., and Laurencin, J., 2024, "Mechanical Response of Carbon Paper Gas Diffusion Layer Under Patterned Compression," Int. J. Hydrogen Energy, **50**(C), pp. 234–247.
[6] Lee, T., and Yang, C., 2020, "A Parametric Study on the Deformation of Gas Diffusion Layer in PEM Fuel Cell," J. Mech. Sci. Technol., **34**(1), pp. 259–268.
[7] García-Salaberri, P. A., Vera, M., and Zaera, R., 2011, "Nonlinear Orthotropic Model of the Inhomogeneous Assembly Compression of PEM Fuel Cell Gas Diffusion Layers," Int. J. Hydrogen Energy, **36**(18), pp. 11856–11870.
[8] Carral, C., and Mélé, P., 2018, "A Constitutive Law to Predict the Compression of Gas Diffusion Layers," Int. J. Hydrogen Energy, **43**(42), pp. 19721–19729.
[9] Afrasiab, H., Davoodi, K. H., Barzegari, M. M., Gholami, M., and Hassani, A., 2022, "A Novel Constitutive Stress-Strain Law for Compressive Deformation of the Gas Diffusion Layer," Int. J. Hydrogen Energy, **47**(75), pp. 32167–32180.
[10] Norouzifard, V., and Bahrami, M., 2014, "Analytical Modeling of PEM Fuel Cell Gas Diffusion Layers Deformation Under Compression: Part 1—Linear Behaviour Region," ECS Trans., **61**(11), pp. 1–12.
[11] Zhang, Z., He, P., Dai, Y.-J., Jin, P.-H., and Tao, W.-Q., 2020, "Study of the Mechanical Behavior of Papertype GDL in PEMFC Based on Microstructure Morphology," Int. J. Hydrogen Energy, **45**(53), pp. 29379–29394.
[12] Sun, Y., Du, P., Bian, M., Miao, H., Hu, H., and Xiao, L., 2015, "Coupling Effects of Microstructure Characteristics on Stress Distribution for Pore-Scale Gas Diffusion Layers," Energies, **18**(7), p. 1561.

[13] Odaya, S., Phillips, R., Sharma, Y., Bellerive, J., Phillion, A., and Hoorfar, M., 2015, "X-Ray Tomographic Analysis of Porosity Distributions in Gas Diffusion Layers of Proton Exchange Membrane Fuel Cells," Electrochim. Acta, **152**, pp. 464–472.
[14] Banerjee, R., and Bazylak, A., 2015, "Three Dimensional, High Resolution MPL Generation for Thermal and Mass Transport Modeling of PEM Fuel Cells," ECS Trans., **69**(17), pp. 121–129.
[15] Fazeli, M., Hinebaugh, J., and Bazylak, A., 2016, "Incorporating Embedded Microporous Layers Into Topologically Equivalent Pore Network Models for Oxygen Diffusivity Calculations in Polymer Electrolyte Membrane Fuel Cell Gas Diffusion Layers," Electrochim. Acta, **216**, pp. 364–375.
[16] Benz, F., 2025, "A Mechanical Model for Carbon Paper Gas Diffusion Layers for Proton Exchange Membrane Fuel Cells Including Fiber and Binder Failure," ASME J. Electrochem. Energy Convers. Storage, **22**(4), p. 041006.
[17] Thiedmann, R., Fleischer, F., Hartnig, C., Lehnert, W., and Schmidt, V., 2008, "Stochastic 3d Modeling of the GDL Structure in PEMFCs Based on Thin Section Detection," J. Electrochem. Soc., **155**(4), p. B391.
[18] Cardiff, P., Karač, A., De Jaeger, P., Jasak, H., Nagy, J., Ivankovic, A., and Tukovic, Z., 2018, "An Open-Source Finite Volume Toolbox for Solid Mechanics and Fluid–Solid Interaction Simulations," preprint arXiv:1808.10736
[19] Silberstein, M. N., and Boyce, M. C., 2010, "Constitutive Modeling of the Rate, Temperature, and Hydration Dependent Deformation Response of Nafion to Monotonic and Cyclic Loading," J. Power Sources, **195**(17), pp. 5692–5706.
[20] Chourdakis, G., Schneider, D., and Uekermann, B., 2023, "Openfoam-Precice: Coupling Openfoam With External Solvers for Multi-physics Simulations," OpenFOAM J., **3**, pp. 1–25.